

INSPIRE: INvestigating Stellar Population In RELics VIII. Emission lines and UV colours in ultra-compact massive galaxies

Chiara Spiniello^{1*}, Mario Radovich², Anna Ferré-Mateu^{3,4}, Roberto De Propris^{5,6}, Magda Arnaboldi⁷,
Francesco La Barbera⁸, Johanna Hartke^{5,9}, Giuseppe D’Ago¹⁰, Crescenzo Tortora⁸, Davide Bevacqua^{11,12},
Michalina Maksymowicz-Maciata¹³, John Mills¹, Nicola R. Napolitano^{14,8}, Claudia Pulsoni¹⁵,
Paolo Saracco¹¹, Diana Scognamiglio¹⁶

¹*Sub-Dep. of Astrophysics, Dep. of Physics, University of Oxford, Denys Wilkinson Building, Keble Road, Oxford OX1 3RH, United Kingdom*

²*INAF - Osservatorio astronomico di Padova, Vicolo Osservatorio 5, I-35122 Padova, Italy*

³*Instituto de Astrofísica de Canarias, Via Láctea s/n, E-38205 La Laguna, Tenerife, Spain*

⁴*Departamento de Astrofísica, Universidad de La Laguna, E-38200, La Laguna, Tenerife, Spain*

⁵*Finnish Centre for Astronomy with ESO (FINCA), FI-20014 University of Turku, Finland*

⁶*Department of Physics and Astronomy, Botswana International University of Science and Technology, Private Bag 16, Palapye, Botswana*

⁷*European Southern Observatory, Karl-Schwarzschild-Straße 2, 85748, Garching, Germany*

⁸*INAF - Osservatorio Astronomico di Capodimonte, Via Moiariello 16, 80131, Naples, Italy*

⁹*Tuorla Observatory, Department of Physics and Astronomy, University of Turku, 20014 Turku, Finland*

¹⁰*Institute of Astronomy, University of Cambridge, Madingley Road, Cambridge CB3 0HA, United Kingdom*

¹¹*INAF - Osservatorio Astronomico di Brera, via Brera 28, 20121 Milano, Italy*

¹²*DiSAT, Università degli Studi dell’Insubria, via Valleggio 11, I-22100 Como, Italy*

¹³*Astrophysics Group, H. H. Wills Physics Laboratory, University of Bristol, Tyndall Avenue, Bristol, BS1 8TL, United Kingdom*

¹⁴*Department of Physics E. Pancini, University Federico II, Via Cinthia 21, I-80126, Naples, Italy*

¹⁵*Max-Planck-Institut für extraterrestrische Physik, Giessenbachstrasse, 85748 Garching, Germany*

¹⁶*Jet Propulsion Laboratory, California Institute of Technology, 4800, Oak Grove Drive - Pasadena, CA 91109, USA*

Last updated 2025 March 26

ABSTRACT

We report the discovery of emission lines in the optical spectra of ultra-compact massive galaxies (UCMGs) from INSPIRE including relics, which are the oldest galaxies in the Universe. Emission-lines diagnostic diagrams suggest that all these UCMGs, independently of their star formation histories, are ‘retired galaxies’. They are inconsistent with being star-forming but lie in the same region of shock-driven emissions or photoionisation models, incorporating the contribution from post-asymptotic giant branch (pAGB) stars. Furthermore, all but one INSPIRE objects have a high [OII]/H α ratio, resembling what has been reported for normal-size red and dead galaxies. The remaining object (J1142+0012) is the only one to show clear evidence for strong active galactic nucleus activity from its spectrum. We also provide near-UV (far-UV) fluxes for 20 (5) INSPIRE objects that match in GALEX. Their $NUV - r$ colours are consistent with those of galaxies lying in the UV green valley, but also with the presence of recently (≤ 0.5 Gyr) formed stars at the sub-percent fraction level. This central recent star formation could have been ignited by gas that was originally ejected during the pAGB phases and then re-compressed and brought to the core by the ram-pressure stripping of Planetary Nebula envelopes. Once in the centre, it can be shocked and re-emit spectral lines.

Key words: Galaxies: evolution – Galaxies: formation – Galaxies: elliptical and lenticular, cD – Galaxies: stellar content – Galaxies: star formation

1 INTRODUCTION

Relic galaxies (Trujillo et al. 2009, 2014; Ferré-Mateu et al. 2017) are the local descendants of high-redshift red nuggets that have completely missed the size-growth evolutionary phase (Daddi et al. 2005; Trujillo et al. 2007; Buitrago et al. 2008; van Dokkum et al. 2008; Naab et al. 2014) and have evolved passively and undisturbed from their first intense and fast high- z star formation (SF) burst. Since

they are made almost exclusively of “in situ” very old stars, like the innermost regions of massive galaxies (e.g., La Barbera et al. 2019; Barbosa et al. 2021) they provide a unique opportunity to track the evolution of this stellar component, which is mixed with the accreted one in normal early-type galaxies (ETGs). They are the ideal systems to investigate and understand the mass assembly in the early Universe with the amount of detail currently available only for galaxies in the local Universe. Moreover, since the number density of relics and its redshift evolution depends strongly on the processes acting during the size growth and how they are modeled, counting relics at low- z is

* Contact e-mail: chiara.spiniello@physics.ox.ac.uk

an incredibly valuable way to disentangle between different galaxy evolution models.

Recent claims have reported the presence of a subpercent fraction of young stellar populations in the innermost region of very massive galaxies and bright cluster galaxies (Salvador-Rusiñol et al. 2021). This is the region where the pristine (i.e., in situ), oldest stars should dominate the light budget (Barbosa et al. 2021). Moreover, the same amount of younger stars ($\sim 1\%$) have also been found in the most extreme relic in the local Universe, NGC 1277 (Salvador-Rusiñol et al. 2022), by fitting near-ultraviolet (NUV) and optical line-strength indices. Since NGC 1277 has not experienced any mergers or interactions with other galaxies, the presence of younger stars in its centre indicates that the gas for the formation of these new stars must be associated with the galaxy itself, i.e., with intrinsic processes rather than external ones. Dopita et al. (2000) highlight that the presence of gas and dust at the centres of passive galaxies may originate from the mass loss of evolved stars. According to their simulation and analysis, in high-pressure interstellar environments like the centres of massive ETGs or UCMGs and relics, the material in the shocked shell of planetary nebulae (PNe) will cool and its expansion reversed, causing a collapse into the denser central region. This will, in turn, recompress the dusty material ejected during the AGB phase of stellar evolution and allow the cold dusty clouds to fall intact (without being destroyed by the hot interstellar medium) towards the nucleus of the galaxy. During this process, the gas could be shocked, creating shock-driven emission lines and, in some cases, form a small percentage of new stars, as in NGC 1277.

The paper is organised as follows. In Section 2 we briefly describe the data used in this paper, highlighting the definition and selection of ultra-compact massive galaxies (UCMGs) and the confirmation of their relic nature. In Section 3 we analyse the emission lines, obtain ratios, and plot diagnostic diagrams to investigate their origins. In Section 4 we focus on the UV, analysing the $NUV-r$ colours. We then discuss the findings and conclude in Section 5 investigating which could be the possible source of both colour and emission lines.

Throughout the paper, we assume a standard Λ CDM cosmology with $H_0=69.6 \text{ km s}^{-1} \text{ Mpc}^{-1}$, $\Omega_\Lambda=0.714$ and $\Omega_M=0.286$ (Bennett et al. 2014).

2 THE SAMPLE

In this paper, we leverage the INvestigating Stellar Population In RELics (INSPIRE, Spiniello et al. 2021b; D’Ago et al. 2023; Spiniello et al. 2024) dataset. INSPIRE is based on an ESO Large Programme that targets 52 spectroscopically confirmed UCMGs at $0.1 < z < 0.4$ with the X-Shooter spectrograph (XSH, Vernet et al. 2011). These objects were initially found in Tortora et al. (2016) from the Kilo Degree Survey (KiDS, Kuijken 2011) third data release (DR3, de Jong et al. 2017), and then spectroscopically confirmed in Tortora et al. 2018 and Scognamiglio et al. 2020 (hereafter T18 and S20, respectively) with low signal-to-noise (SNR) and medium-resolution optical spectra. For each galaxy, structural parameters and stellar masses have been derived from $ugri$ KiDS photometry (Roy et al. 2018; Tortora et al. 2018; Scognamiglio et al. 2020). All objects are UCMGs in the sense that they are clear outliers in the stellar mass-size plane (see Fig. 2 in Spiniello et al. 2021a), having very small sizes (with effective radii $R_e < 2 \text{ kpc}$) with respect to the overall population of passive galaxies with relatively large stellar masses ($M_\star > 6 \times 10^{10} M_\odot$). Stellar masses and sizes for the entire INSPIRE sample are provided in Table 1 of Spiniello et al. (2024, hereafter S24).

From UVB-to-NIR high-resolution, medium signal-to-noise (SNR) spectra¹ we have measured the integrated stellar kinematics (D’Ago et al. 2023), as well as stellar population age, metallicity, [Mg/Fe] abundances and the IMF slope (Martín-Navarro et al. 2023; Maksymowicz-Maciata et al. 2024). Of these UCMGs, 38 have been classified as relics, since they formed more than 75% of their stellar masses already by $z > 2$ (Spiniello et al. 2021b, 2024). Hence, INSPIRE has enlarged by at least a factor of 5 the number of nearby fully confirmed relics, providing the first statistically significant sample of these objects. Here, we focus on optical emission lines and UV colours, aiming at investigating on their sources and on whether a correlation exists between UV-light, emission lines and the *degree of relicness* (DoR). The DoR is a dimensionless number ranging from 0 (non relic) to 1 (extreme relic), that quantifies how extreme and peaked the SFH of these UCMGs is. We refer the reader to Spiniello et al. (2024, hereafter S24) for more details on how the DoR is computed.

We use here the 52 INSPIRE UVB+VIS XSH spectra to measure emission lines, as described in the next section.

3 EMISSION LINES

In roughly half of the spectra released in the third INSPIRE data release (DR3, S24), we observe convincing evidence for emission lines from [OII] ($\lambda \sim 3727\text{\AA}$) and [NII] ($\lambda \sim 6583\text{\AA}$) in the combined UVB+VIS spectra. This is broadly consistent with the statistics, based on a much larger sample of normal-sized galaxies ($\sim 300,000$ galaxies from SDSS DR4, Adelman-McCarthy et al. 2006), of Yan et al. (2006): 38% of all red galaxies have detectable [OII] emission.

Weak emissions are also detected in [OIII] ($\lambda \sim 5007\text{\AA}$) and [SII] ($\lambda \sim 6720\text{\AA}$). Finally, $H\beta$ and $H\alpha$ also have very weak emission components in some cases, although they are contaminated by stellar absorption lines. No other emission lines are detected in the wavelength range $[2700-9500]\text{\AA}$.

Unfortunately, the SNRs of most emission lines are generally low (≤ 10), with the exception of J1142+0012 (which will be discussed later). Moreover, the continuum underlying [OII] has many narrower absorption features that could bias the measurement of the flux. Hence, to compute the equivalent width (EW) of the line and flux in emission, we first subtract the stellar component and then perform a fit to the emission lines.

To compute EWs and fluxes, we use a Python code, based on the LMFIT library², that fits emission lines with Gaussian profiles. We also note that for [OII]($\lambda 3736,29$), $H\alpha$ + [NII]($\lambda 6548,83$) and [SII]($\lambda 6716,31$), the fit is performed using several Gaussians simultaneously. However, in order to ensure that the results are based only on reliable measurements, we consider only lines with an $\text{SNR} > 2$ and a FWHM $> 1\text{\AA}$.

The fluxes of all emission lines that pass the above thresholds are provided in the central block of columns in Table 1, along with their uncertainties, in units of $10^{-17} \text{ erg s}^{-1} \text{ cm}^{-2} \text{\AA}^{-1}$. We note that the velocity dispersion of the emission lines is similar to that of the stars, which disfavour an origin due to AGN or extreme shock waves.

In the following, we will make use of line-line plots and emission line diagnostic to investigate the possible origin of emission in UCMGs and relics.

¹ Publicly available through the ESO Phase 3 Science Archive

² <https://lmfit.github.io/lmfit-py/>

GALAXY ID	DoR	[OII]	H β	[OIII]	H α	[NII]	[SII]	FUV (mag)	NUV (mag)	NUV-r
		$\lambda 3727 + 3729$	$\lambda 4861$	$\lambda 5007$	$\lambda 6563$	$\lambda 6583$	$\lambda 6717 + 6731$			
J0211-3155	0.72	0.72 ± 0.19	0.57 ± 0.21	0.50 ± 0.18	–	–	–	–	23.42	3.64
J0224-3143	0.56	–	–	–	–	–	–	–	–	–
J0226-3158	0.12	–	–	1.21 ± 0.35	–	–	–	–	23.27	4.02
J0240-3141	0.43	0.87 ± 0.21	0.72 ± 0.42	2.23 ± 0.73	–	–	–	–	–	–
J0314-3215	0.42	2.03 ± 0.21	0.59 ± 0.28	1.47 ± 0.46	1.09 ± 0.27	1.90 ± 0.31	1.34 ± 0.24	–	–	–
J0316-2953	0.40	1.36 ± 0.19	–	–	–	1.55 ± 0.30	–	–	22.87	3.21
J0317-2957	0.51	–	–	–	–	–	–	–	–	–
J0321-3213	0.37	6.10 ± 0.34	1.03 ± 0.32	1.02 ± 0.34	3.40 ± 0.30	4.27 ± 0.34	–	–	–	–
J0326-3303	0.25	–	0.84 ± 0.28	–	–	–	–	–	–	–
J0838+0052	0.54	1.39 ± 0.18	–	–	–	1.18 ± 0.30	–	–	–	–
J0842+0059	0.73	2.72 ± 0.22	2.10 ± 0.53	0.77 ± 0.34	1.24 ± 0.28	2.00 ± 0.32	–	–	–	–
J0844+0148	0.45	1.32 ± 0.21	–	2.42 ± 0.68	1.26 ± 0.30	2.09 ± 0.36	–	–	22.26	2.48
J0847+0112	0.83	5.09 ± 0.25	0.94 ± 0.69	3.30 ± 0.97	3.18 ± 0.46	3.15 ± 0.48	4.72 ± 0.71	–	23.40	4.99
J0857-0108	0.39	–	–	0.83 ± 0.21	–	–	–	–	24.07	4.86
J0904-0018	0.32	–	–	–	–	–	–	23.17	22.20	3.09
J0909+0147	0.79	4.74 ± 0.64	2.55 ± 0.76	–	–	–	–	–	–	–
J0917-0123	0.44	2.79 ± 0.23	0.69 ± 0.32	1.59 ± 0.29	3.17 ± 0.35	5.36 ± 0.41	4.43 ± 0.54	–	–	–
J0918+0122	0.43	–	0.83 ± 0.49	–	–	1.86 ± 0.46	–	–	24.12	4.99
J0920+0126	0.25	–	–	0.85 ± 0.29	–	0.72 ± 0.28	–	–	–	–
J0920+0212	0.64	–	–	3.03 ± 0.97	–	–	–	22.77	22.27	3.40
J1026+0033	0.29	4.17 ± 0.50	–	4.65 ± 1.77	–	4.11 ± 1000.00	–	22.92	21.58	4.19
J1040+0056	0.77	6.05 ± 0.18	–	4.44 ± 0.38	2.62 ± 0.40	2.76 ± 0.42	3.89 ± 0.34	–	–	–
J1114+0039	0.40	–	–	–	–	–	–	–	–	–
J1128-0153	0.34	1.47 ± 0.32	–	2.28 ± 0.44	–	–	–	–	23.29	4.73
J1142+0012	0.18	46.05 ± 2.23	21.16 ± 0.76	173.99 ± 4.94	93.04 ± 4.27	162.70 ± 4.90	88.35 ± 3.59	21.97	21.34	4.32
J1154-0016	0.11	–	–	–	–	–	–	–	23.71	4.19
J1156-0023	0.30	2.50 ± 0.24	1.18 ± 0.58	2.63 ± 0.79	–	2.10 ± 0.57	–	–	–	–
J1202+0251	0.36	–	–	–	–	–	–	–	–	–
J1218+0232	0.45	3.47 ± 0.24	–	2.07 ± 1.94	1.66 ± 0.33	2.68 ± 0.38	–	–	23.23	4.00
J1228-0153	0.39	2.07 ± 0.29	0.91 ± 0.35	0.78 ± 0.36	–	1.36 ± 0.34	–	–	–	–
J1402+0117	0.31	1.08 ± 0.14	1.10 ± 0.41	1.16 ± 0.42	1.14 ± 0.22	1.33 ± 0.24	–	–	–	–
J1411+0233	0.41	1.54 ± 0.22	–	–	–	–	–	–	–	–
J1412-0020	0.61	–	–	–	–	–	–	–	22.54	3.35
J1414+0004	0.36	3.09 ± 0.34	1.20 ± 0.91	1.41 ± 0.32	1.71 ± 0.32	3.85 ± 0.38	–	–	–	–
J1417+0106	0.33	–	–	0.65 ± 0.38	–	–	–	–	–	–
J1420-0035	0.41	–	–	1.07 ± 0.59	–	–	2.39 ± 0.55	–	–	–
J1436+0007	0.33	4.15 ± 0.35	–	–	2.75 ± 0.33	4.21 ± 0.36	2.43 ± 0.46	–	–	–
J1438-0127	0.78	0.83 ± 0.15	0.65 ± 0.28	1.64 ± 0.35	–	1.22 ± 0.28	–	–	–	–
J1447-0149	0.38	4.94 ± 0.34	1.99 ± 0.65	3.05 ± 0.66	3.21 ± 0.35	4.75 ± 0.39	3.45 ± 0.48	–	23.32	4.71
J1449-0138	0.60	–	0.65 ± 0.33	0.34 ± 0.14	0.52 ± 0.16	–	–	–	–	–
J1456+0020	0.17	4.06 ± 0.20	1.06 ± 0.60	0.88 ± 0.37	2.10 ± 0.29	4.26 ± 0.35	–	23.02	23.18	3.72
J1457-0140	0.47	–	–	–	–	–	–	–	23.53	4.10
J1527-0012	0.38	–	–	–	–	–	–	–	–	–
J1527-0023	0.37	2.26 ± 0.21	–	–	–	2.51 ± 0.62	–	–	23.99	4.35
J2202-3101	0.48	2.66 ± 0.19	2.30 ± 0.79	2.28 ± 0.50	2.62 ± 1.00	3.23 ± 1.11	–	–	–	–
J2204-3112	0.78	–	1.05 ± 0.37	0.44 ± 0.16	–	–	–	–	–	–
J2257-3306	0.27	–	–	0.59 ± 0.24	–	–	–	–	–	–
J2305-3436	0.80	–	–	0.45 ± 0.26	–	–	–	–	–	–
J2312-3438	0.36	–	–	0.53 ± 0.18	–	–	–	–	–	–
J2327-3312	0.06	3.96 ± 0.14	–	2.57 ± 0.25	2.34 ± 0.28	4.65 ± 0.34	3.00 ± 0.73	–	–	–
J2356-3332	0.44	2.41 ± 0.15	1.27 ± 0.40	1.94 ± 0.39	1.03 ± 0.32	1.07 ± 0.32	–	–	23.27	3.46
J2359-3320	0.71	–	–	2.79 ± 1.00	–	–	–	–	–	–

Table 1: Emission lines fluxes for the INSPIRE galaxies. For each object, we give ID and DoR (computed in S24) in the first block of columns, the flux with uncertainties of all the lines we use in this letter in the second block, and GALEX observed magnitudes and the $NUV - r$ colour in the third block. Missing measurements are not passing the thresholds described in Sec. 3. Units for spectra are in 10^{-17} erg s $^{-1}$ cm $^{-2}$ Å $^{-1}$.

3.1 [OII]/H α bimodality

Yan et al. (2006, hereafter Y06) reported the discovery of a bimodality in [OII]/H α ratio among $\sim 300,000$ galaxies from the fourth SDSS Data Release (DR4; Adelman-McCarthy et al. 2006). One mode is largely associated with star-forming galaxies, while the other mode contains galaxies with line ratios compatible with low-ionisation nuclear emission-line regions (LINERs). Narrow-line Seyferts and

transition objects mostly fall in between the two dominant populations, consistent with the picture that both SF and AGNs (or some other sources, e.g. pAGBs) might contribute substantially to the emission in these objects. In Figure 1, we reproduce the $\log([OII]_{EW}) - \log(H\alpha_{EW})$ diagnostic plot used by Y06 for the INSPIRE galaxies³

³ Note that, in Figure 1, we plot the EWs of the lines, rather than their fluxes.

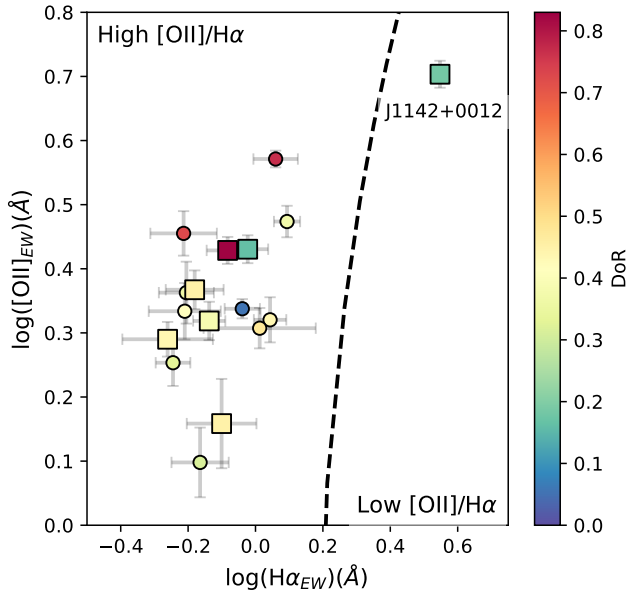


Figure 1. The distribution of INSPIRE galaxies in $\log H\alpha - \log[\text{OII}]$ EWs, and colour-coded by DoR. Objects on the left side of the black dashed lines are classified as ‘High $[\text{OII}]/H\alpha$ ’. The only ‘Low $[\text{OII}]/H\alpha$ ’ galaxy from the INSPIRE sample is J1142+00122, which shows clear sign of AGN activity in its spectrum. Squares denote objects with a match in GALEX.

to check whether a bimodality exists also in this sample (i.e., with objects with higher DoR falling in the LINERs region while nonrelic UCMGs being more compatible with star-forming galaxies).

All but one object are classified as ‘High $[\text{OII}]/H\alpha$ ’ galaxies, according to the threshold set by Eq. 6 in Y06. Indeed, Y06 showed that the bimodality in $[\text{OII}]/H\alpha$ ratio echoes the galaxies’ colour bimodality and the great majority of red galaxies reside in the ‘High $[\text{OII}]/H\alpha$ ’ category. Moreover, even though, in theory, SF models can explain a high $[\text{OII}]/H\alpha$ ratio, they would predict much lower $[\text{NII}]/[\text{OII}]$ ratios (for solar or supersolar metallicities) than the one observed for the INSPIRE sample (Gutkin et al. 2016).

The only system classified as ‘Low $[\text{OII}]/H\alpha$ ’ is J1142+0012 (DoR = 0.18, i.e. nonrelic). This is the only INSPIRE object that has a spectrum consistent with a Seyfert 1 AGN, with broad and strong $H\alpha$ emission. This system will be further investigated in an upcoming publication. The three extreme relics for which a secure measurement of the $[\text{OII}]$ and $H\alpha$ lines is possible seem to have a higher $\log([\text{OII}]_{EW})$ than objects with lower DoR. However, unfortunately, we do not have a large enough sample to draw firm conclusions.

3.2 BPT and WHAN diagnostic diagrams

We use the classical emission-line diagnostics diagram (Baldwin et al. 1981; Rola et al. 1997; Kauffmann et al. 2003) to further investigate on the possible source generating emission lines in red UCMGs, including in those classified as relics ($0.34 < \text{DoR} < 0.7$) and extreme relics ($\text{DoR} \geq 0.7$). This approach effectively differentiates between a star-forming (SF) and an active galactic nucleus (AGN) origin by examining the ratios of various emission lines. We start by producing the classical ‘Baldwin, Phillips & Terlevich’ (BPT) diagrams (Baldwin et al. 1981). In these diagrams, two main tracks of galaxies are visible and separate. Star-forming objects will dominate the left-bottom region, whereas ‘AGN-like’ objects will lie on the right side. Traditionally, AGNs can then be further divided into subcategories

occupying different positions in the diagrams: Seyfert galaxies in the upper part and LINERs towards the bottom region. Both theoretical and empirical classifications have been reported in the literature (e.g. Kewley et al. 2001, 2004, 2006; Kauffmann et al. 2003). In the upper panel of Figure 2 we show these diagrams for the INSPIRE objects where emission lines are securely detected, again colour-coded by their DoR. The large uncertainty on the $H\beta$ emission, mainly due to the low SNR in the blue, prevents us from obtaining an estimate of the extinction from the Balmer decrement. For comparison, in the same panel, we also show the line ratios produced by SF models with an age ≤ 3 Myr, corresponding to ionisation by OB stars (grey dots). Clearly, the INSPIRE objects are not well reproduced by SF models, having a too high $[\text{NII}]/H\alpha$ and $[\text{SII}]/H\alpha$ ratios. The SF models could still reproduce the observed $[\text{OII}]/H\alpha$ ratio (up to $\log [\text{OII}]/H\alpha = 0.32$, the maximum value allowed by the SF models, as shown by the vertical dotted line in Figure 2), but only if no correction for internal dust extinction is considered. For instance, $H\alpha/H\beta=4$ would correspond to a correction of +0.27. The UCMG line ratios can instead be reproduced by shock and/or photoionisation models that include the contribution of pAGB stars, as shown in the middle and low panels of Figure 2.

First, we consider the shock models from Alarie & Morisset (2019), available in the Mexican Million Database (3MdB: Morisset et al. 2015)⁴. The models were derived using the MAPPINGS V code (Sutherland & Dopita 2017), which allows us to retrieve emission lines produced in a shocked gas, both with and without the presence of the so-called precursor⁵. The middle panel of Figure 2 displays the line ratios produced by the shock models with parameters as described in Allen et al. (2008). In particular, we consider:

- only pure shock models, since adding the precursor would produce $[\text{OIII}]/H\beta$ ratios much higher than the value observed in INSPIRE UCMGs;
- models with solar ($Z = 0.0183$, blue and light blue) and twice solar ($Z = 0.0358$, red) metallicities;
- models with shock velocities v_{sh} with values between 100 km s^{-1} (small points) and 500 km s^{-1} (big circle);
- pre-shock densities of $n_0 = 1 \text{ cm}^{-3}$ (light blue) and $n_0 = 1 \text{ cm}^{-3}$ (blue) for the solar metallicity models and $n_0 = 1 \text{ cm}^{-3}$ (the only available) for the super-solar models;
- models with transverse magnetic fields of 10^{-4} , 1, 5, 10 $\mu\text{G cm}^{3/2}$.

Secondly, we use the models by Martínez-Paredes et al. (2023, MP23 hereafter) who recently presented a large set of photoionisation models, which are publicly available in the CB_19 table of 3MdB. We refer to MP23 for details of how the models were computed and the description of their parameters. In short, the photoionisation code CLOUDY (Ferland et al. 2017, v. 17.03) has been used to compute emission line ratios adopting as a ionising source the population synthesis models described in Plat et al. (2019) and Sánchez et al. (2022) that include the contribution from pAGB stars (also defined as HOLMES: hot low-mass evolved stars). We select from the MP23 models the ones that give line ratios close to those measured in the INSPIRE galaxies. They are displayed in the bottom panel of Figure 2, where the models are chosen to have the following:

- a single stellar population (SSP) with a Kroupa IMF up to 100 solar masses (RB–SSP–Kroup–MU100) and an age of 1 Gyr as the

⁴ <https://sites.google.com/site/mexicanmillionmodels/>

⁵ The precursor is where the gas entering the shock is photoionised by the UV radiation emitted by the shocked gas.

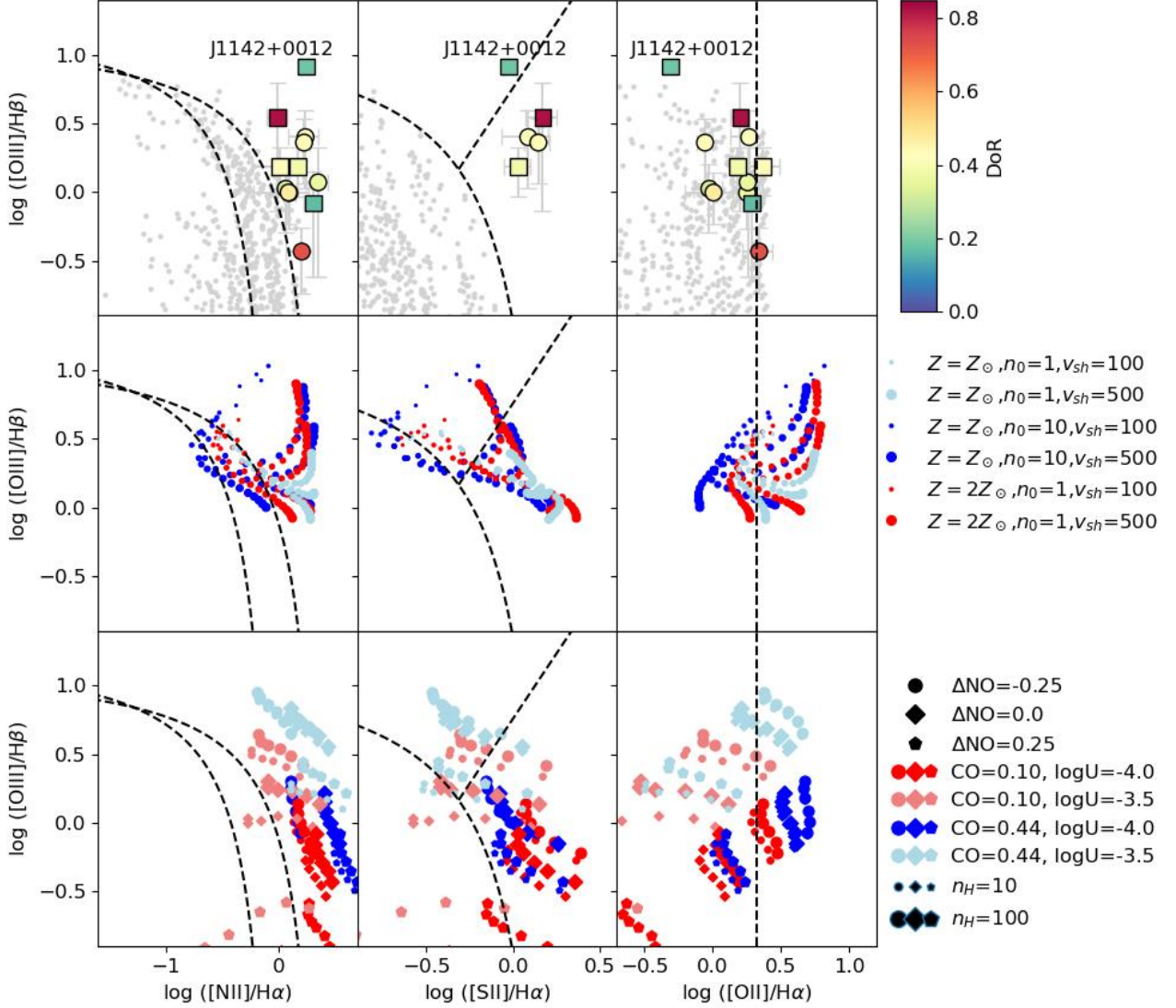


Figure 2. The BPT diagrams with the classifying scheme (dashed lines, from left to right): SF demarcations from Kewley et al. (2001); Kauffmann et al. (2003); SF (Kewley et al. 2001) and AGN/LINER (Kewley et al. 2006) demarcations; maximum SF value (Kewley et al. 2004). *Top*: The line ratios of INSPIRE points, colour-coded by the DoR, on top of predictions from SF models (grey dots). Squares are galaxies with a match in GALEX. *Middle*: Emission line ratios from the shock models by Alarie & Morisset (2019) with the parameters as described in the legend and in the text. *Bottom*: Emission line ratios from the MP23 photoionization models with parameters as shown in the legend.

ionising source. However we note that similar line ratios would be obtained changing the age of the models up to 10 Gyr;

- metallicity of $Z = 0.03$ ($[M/H]=0.22$), as from the stellar population analysis performed in S24 we conclude that UCMGs are consistent with super-solar metallicities. We note that selecting models with solar metallicities would produce BPT ratios only slightly shifted to the SF region;

- an ionization parameter $\log U < -3$;

- a density $n_H = [10, 100] \text{ cm}^{-3}$;

- values of the $H\beta$ fraction defining the thickness of the ionized cloud between 0 and 1;

- CNO gas abundances: $C/O=[0.1, 0.44]$, $\Delta N/O=[-0.25, 0, 0.25]^6$, $12+\log \text{OH}=9.14$.

With the exception of J1142+0012, models with ionisation dominated by pAGB stars allow to reproduce well the emission line ratios observed in the INSPIRE UCMGs. Nevertheless, as shown by Stasińska et al. (2008) and further discussed by Cid Fernandes et al. (2011), retired galaxies (i.e. emission-line galaxies that have stopped forming stars and are ionised by hot low-mass evolved stars) have the same location in the BPT diagram as galaxies hosting weak AGNs.

⁶ Defined in MP23 as the deviation from the (N/O) to (O/H) ratio as defined in Gutkin et al. (2016)

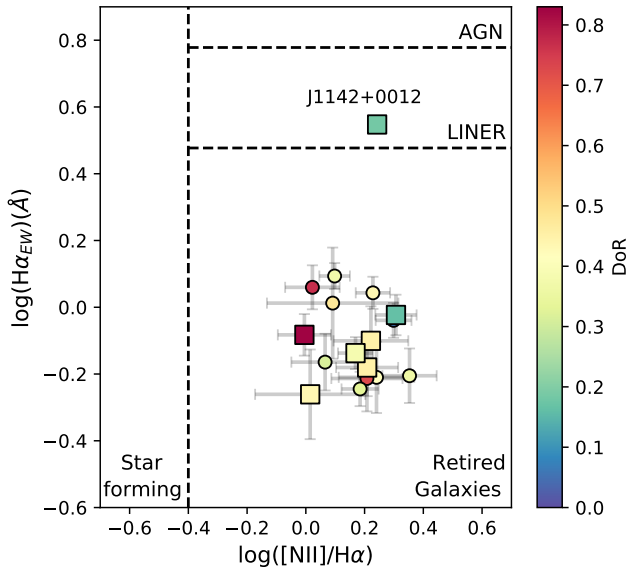


Figure 3. The WHAN diagram (Cid Fernandes et al. 2011) for the INSPIRE galaxies, colour-coded by their DoR. Squares are objects with a match in GALEX. Dashed lines separate SF from LINERs and AGNs. The only system consistent with being a LINER is J1142+0012.

According to Lee et al. (2024), photoionisation by pAGB stars and interstellar shocks can only be distinguished with in-depth analysis, for instance using temperature predictions.

To try to more precisely separate pure SF galaxies, AGN hosts (strong and weak) and passive galaxies (i.e. retired, red and dead galaxies) we use the so-called WHAN diagram (Cid Fernandes et al. 2011) showing the [NII]/H α ratio against the H α EW. This is plotted in Figure 3 for the INSPIRE galaxies for which we could measure H α and [NII] emissions with high confidence. Here, all galaxies with reliable emission lines but J1142+0012 lie in the ‘retired galaxies’ region, hence completely ruling out SF and disfavours an AGN origin as the most probable source of emission lines in UCMGs and relics (with no DoR dependency). We therefore argue that the emission lines in INSPIRE UCMGs can be explained by either the presence of pAGB stars or shocks of the gas produced by the mass loss of evolved stars, which collects at the centres of the UCMGs.

4 UV DETECTION

To acquire an independent line of evidence on the possible origin of emission lines, in this section we look at the UV fluxes for INSPIRE objects. Unfortunately, the SNR of X-Shooter spectra of single galaxies is too low in the UV. Hence, to investigate whether the INSPIRE UCMGs have detectable UV fluxes, we cross-match the INSPIRE catalogue with data from the Galaxy Evolution Explorer (Morrissey et al. 2007), matching sources to GALEX photometry within $10''$. We caution the reader that the spatial resolution of GALEX is sub-optimal when matching ultracompact galaxies, with sizes smaller than the nominal survey resolution (FWHM $\approx 6''$). However, we checked that no other source was present within this radius in the u band images from SDSS or the g band images from PanStarrs. Thus, we are confident that the detected emission comes from the UCMGs themselves.

Among the 52 INSPIRE objects, 20 have a match, with near-UV (NUV) magnitudes ranging between 21.3 and 24.1, and spanning a

wide range of DoR, from nonrelics (DoR < 0.34) with an extended SFH, to extreme relics (DoR ≥ 0.7) that have assembled all their stellar mass within the first 2 Gyr after the Big Bang (S24). In addition, 5 UCMGs have also been detected in the far-UV (FUV) but only one of them is a relic, according to the INSPIRE classification (J0920+0212, DoR = 0.64). The final block of columns of Table 1 provides FUV and NUV magnitudes, as well as $NUV - r$ colours.

The top panel of Figure 4 shows the $NUV - r$ colour⁷ versus the DoR for the 20 detected objects. We also plot the objects without a match in GALEX as black crosses at the top of the panel to show that, perhaps surprisingly, no correlation with the DoR is found. The galaxies’ colours lie perfectly in between the mean colour computed by Ardila et al. (2018, Tab. 1) for red and dead (quiescent) galaxies (4.54 ± 1.00 , red-shaded region) and the mean colour estimated for Active Galactic Nuclei (AGNs, 2.48 ± 1.24 , yellow-shaded region). They are consistent with the UV green valley (Salim 2014) and lie at the redder end of those measured in post-starburst galaxies where the UV flux is mainly caused by intermediate-age pAGB stars (Melnick & De Propris 2013). The $NUV - r$ colour of the matched INSPIRE objects are instead generally redder than these computed for star-forming galaxies (2.01 ± 0.68 , Ardila et al. 2018).

However, another equally valid scenario can reproduce the $NUV - r$ colour of the INSPIRE objects. Indeed, they can be perfectly fitted with an overall old stellar population plus the addition of a small percentage of young stars, as suggested by Salvador-Rusiñol et al. (2021). This is shown in the bottom panel of Figure 4 where we plot predictions on the $NUV - r$ colour obtained from the E-MILES single stellar population models (SSPs, Vazdekis et al. 2016). In particular, we computed the expected colour for an old stellar population (10 Gyr) with solar metallicity to which a small percentage (< 5 %) of young stars (≤ 0.5 Gyr) is added, also with solar metallicity⁸. We explore the colour variation due to changes in age and metallicity of the main old population, finding negligible effects on the main conclusions.

Importantly, we point out that the presence of a sub-percentage population of young stars is not in disagreement with our analysis of the main ionisation mechanism of emission lines (Sec. 3). In fact, the latter constrains the presence of SF on a much shorter time scale (of the order of few Myr) compared to UV colours.

To further address this issue, we estimate the star formation rate (SFR) for the only six systems with a match in GALEX and a measured H α emission (J0844+0148, J0847+0112, J1218+0232, J1447-0149, J1456+0020, J2356-3332)⁹. First, we convert the H α flux into a total luminosity, considering it unresolved, as the spectra are fully seeing-dominated (see S24). Second, we translate H α luminosities into SFRs following Kennicutt (1998). In particular, we use Equation 12 and Table 1 of Kennicutt & Evans (2012):

$$\log \dot{M}_{\star} [M_{\odot} \text{yr}^{-1}] = \log(L_{H\alpha}) - \log C_x \quad (1)$$

where $\log C_x = 41.27$ (Murphy et al. 2011). The resulting SFRs for the six systems range between 0.01 and 0.02 $M_{\odot} \text{yr}^{-1}$.

At this point, we compute the stellar mass that would be formed in ~ 0.5 Gyr (the oldest age of the young stellar population component in Figure 4) with a constant rate of star formation of 0.02 $M_{\odot} \text{yr}^{-1}$ (as inferred from H α), finding that it would be of the order of $M_{\star, H\alpha} \sim$

⁷ Optical r -band magnitudes have been retrieved from KiDS DR4 (Kuijken et al. 2019).

⁸ We stress that this assumption does not change the results as the effect of changing the metallicity on the $NUV - r$ colour is negligible.

⁹ Excluding J1142+0012 which is an AGN.

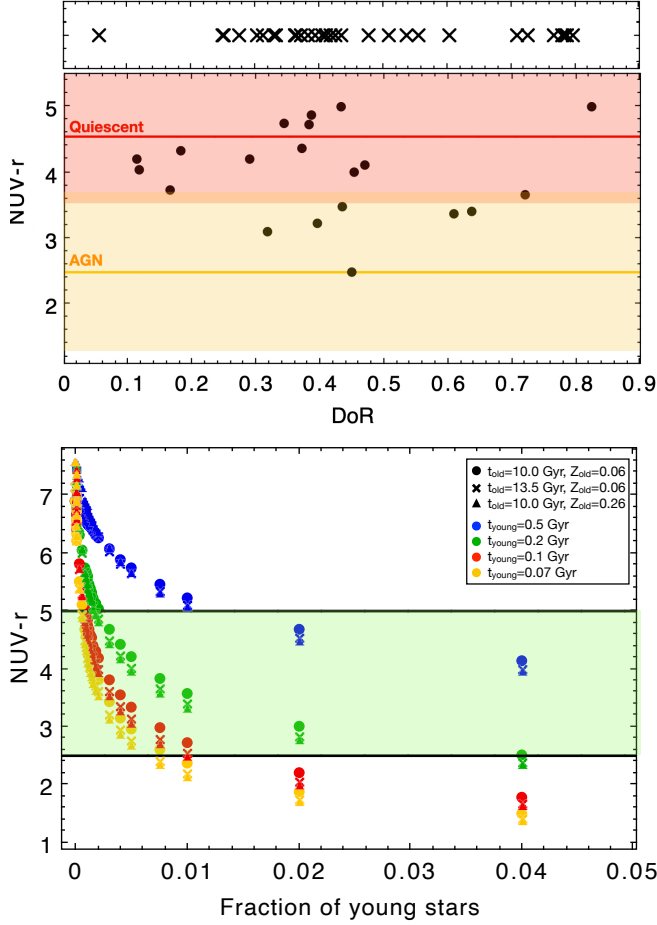


Figure 4. *Top:* $NUV - r$ colour for the INSPIRE galaxies with a detection in GALEX plotted versus their DoR. On the top, black crosses indicate objects without a match to show that both detection and non-detection cover a wide range of DoR. The red and yellow lines (and shaded regions) indicate the mean colour (and standard deviation) for quiescent and AGNs, respectively (Ardila et al. 2018). *Bottom:* $NUV - r$ prediction from E-MILES SSP (Vazdekis et al. 2016) old models with a small percentage of younger stars, as reported in the legend. The green shaded region shows the $NUV - r$ range covered by INSPIRE galaxies.

$10^7 M_{\odot}$. This is also in agreement with empirical relations (e.g., Elbaz et al. 2007) and simulations (e.g., Ciesla et al. 2017) predicting that SFRs < 0.1 correspond to $M_{\star} < 10^8 M_{\odot}$. In Figure 4, the fraction of young stars required to explain the $NUV - r$ colour depends significantly on the age of the young component, ranging from ~ 0.001 ($t_{\text{young}} = 0.07$ Gyr) to ~ 0.04 ($t_{\text{young}} = 0.5$ Gyr). Hence, since the typical mass of INSPIRE objects is $M_{\star} \geq 6 \times 10^{10} M_{\odot}$, this implies a stellar mass in the young component $M_{\star, NUV-r} \geq 6 \times 10^7 M_{\odot}$.

In conclusion, since $M_{\star, NUV-r} > M_{\star, H\alpha}$, even assuming that all the $H\alpha$ emission comes from newly formed stars ($10^7 M_{\odot}$), this is not enough to explain the $NUV - r$ colour¹⁰. However, we must

¹⁰ We note that we did not apply any correction for extinction. However, for the 5 systems for which $H\beta$ emission is also measured, the SFRs can increase up to a factor of 3, given that the Balmer decrement values range between ~ 1 and ~ 5 (although with very large uncertainties on $H\beta$). This is still not enough to explain the $NUV - r$ colours through the $H\alpha$ fluxes.

stress a couple of important points. First, the assumption of a constant SFR might not be correct. Indeed, the SFR could decrease with time or even more likely occur in a bursty fashion (e.g., due to residual AGN activity), which would make extremely hard to detect it on very short timescales as those probed by $H\alpha$ ($\lesssim 10$ Myr). Secondly, in the case of a non-universal IMF, within the integrated galactic stellar initial mass function (IGIMF) theory (Kroupa & Weidner 2003), i.e. assuming that the IMF slope steepens with decreasing SFR, the ionising photons that produce $H\alpha$ emission would be significantly lower, given the smaller number of massive stars, than for a standard IMF, meaning that the above value of $M_{\star, H\alpha}$ might be significantly underestimated.

5 DISCUSSION AND CONCLUSIONS

In this paper we have reported the detection of emission lines and significant NUV emission in the UVB+VIS spectra of about half of the INSPIRE UCMGs, including some of the most extreme relics.

The [OII] emission line, which is the strongest that we detect in the INSPIRE galaxies, has been widely used in the literature as an empirical SF rate indicator, calibrated through comparison with Hydrogen lines (e.g. Gallagher et al. 1989; Rosa-González et al. 2002; Kewley et al. 2004). However, the situation is controversial as the same emission line, and others such as [NII] and $H\alpha$, have been detected in spectra of red and dead elliptical galaxies at different redshifts (Caldwell 1984; Yan et al. 2006; La Barbera et al. 2019; Maseda et al. 2021), where SF is not expected. Another possible origin for emission lines in red ETGs comes from the photo-ionisation by exposed cores of evolved stars with ages greater than 100 Myr, such as pAGBs (Greggio & Renzini 1990; Binette et al. 1994; Yan & Blanton 2012; Papaderos et al. 2013; Belfiore et al. 2016) and PNe (Taniguchi et al. 2000). Alternatively, AGNs and especially LINERs, fast shock waves, and cooling flows might also produce [OII] emission (Ferland & Netzer 1983; Halpern & Steiner 1983; Dopita & Sutherland 1995; Groves et al. 2004). Hence, we have analysed the emission line ratios to understand what is most likely causing them in the ‘building blocks’ of massive ETGs, the oldest and densest galaxies in the nearby Universe.

We find emission lines for galaxies at all DoR, including some of the most extreme relics. All but one object (J1142+0012) have a high [OII]/ $H\alpha$ ratio, typical of red and dead galaxies (Y06). La Barbera et al. (2019) also found strong [OII] emission in the core of massive, giant ETGs with very old stellar populations, the region where the ‘pristine’ stellar population dominates the light. A high [OII]/ $H\alpha$ is characteristic of ‘retired galaxies’ (Y06) and this conclusion is further corroborated by the lack of clear and strong $H\alpha$ emission, which is still present in a number of systems but very weak. In BPT and WHAN diagrams, the line ratio of INSPIRE objects cannot be reproduced by SF models. Hence, we fully exclude that the main ionisation mechanism is on-going star formation. Line ratios are, instead, fully consistent with those predicted by shock models (Alarie & Morisset 2019) and by models that include the contribution from HOLMES stars (Martínez-Paredes et al. 2023). Both of these scenarios advocate for internal and passive processes, rather than external or environmental ones (e.g., mergers or interactions). Importantly, this opens up new insights into the understanding of the mass assembly and cosmic evolution of the local massive ETGs.

We also looked at the $NUV - r$ colours for the 20 INSPIRE galaxies with a match in GALEX. They are very similar to those measured for post-starburst galaxies (Melnick & De Propris 2013). This may hint at the UV emission being powered by the same mechanisms

(evolved stars) plus, possibly, some AGN contribution (Ardila et al. 2018), which is, however, disfavoured by the line ratio analysis. It should also be pointed out that the timescales for the SF traced by emission lines and UV colours are different. In addition, the INSPiRE $NUV - r$ colour can be reproduced with an overall old population (~ 10 Gyr) plus a sub-percent young population (~ 0.1 - 0.5 Gyr). Given also the very recent results on NGC 1277 (Salvador-Rusiñol et al. 2022) where this is indeed demonstrated from UV and VIS line-index analysis, we cannot exclude that the UV colours are due, at least partially, to a sub-percent contribution of star formation. In this case, since the relics did not interact with any other galaxy after the very first assembly phase at high- z , the emissions (and the possible residual SF causing blue UV colours) must have been caused by intrinsic processes. One possible scenario able to explain all the lines of evidence presented here is the one outlined in Dopita et al. (2000). The authors attribute the origin of the gas in the centres of red and dead massive ETGs to the mass loss due to evolved stars. In particular, pAGBs and PNe, which share the velocity dispersion of the native stellar population, give the largest contribution to the gas mass. A simple calculation, which assumes the PN birth rate of ($\dot{\epsilon} \approx 4 \times 10^{-12} \text{ yr}^{-1} L_{\odot}^{-1}$, Mendez & Soffner 1997), the typical luminosity and size of UCMGS ($L \approx 6 \times 10^{10} L_{\odot}$, $R_e \leq 1.7$ kpc), and the amount of mass loss by each PN to the interstellar medium (ISM), $\sim 0.4 M_{\odot}$, leads to a gas loss rate by all the PNe of about $0.24 M_{\odot} \text{ yr}^{-1}$. This means that in less than 10^9 years, they can feed more than $10^8 M_{\odot}$ of gas and dust into the UCMGS. This gas, given the high relative motion of the PN envelopes through the ISM of such very dense stellar systems with high stellar velocity dispersion ($> 200 \text{ km s}^{-1}$, D'Ago et al. 2023), does not evaporate but collapses in dense clouds. These then infall radially towards the centre, where they can be shocked, possibly causing emission lines, and heated, therefore forming new stars at a sub-percentage level.

The analysis we presented here allowed us to completely exclude that the emission lines are caused by star formation, but it is unfortunately unable to disentangle between shock-driven emission or pAGBs stars. Furthermore, a small contribution from the central AGN is still possible, although disfavoured. The only way forward in this sense is to obtain high spatial resolution spectroscopy and (far and near) UV-deep imaging to be able to resolve the stellar populations and the internal structure of the most compact and dense massive galaxies in the nearby Universe.

ACKNOWLEDGEMENTS

We acknowledge the usage of the Mexican Million Database (Morisset et al. 2015). CS, CT, FLB, DB, and PS acknowledge funding from the INAF PRIN-INAF 2020 programme 1.05.01.85.11. JH and CS acknowledge the financial support from the mobility programme of the Finnish Centre for Astronomy with ESO (FINCA), funded by the Academy of Finland grant nr 306531. AFM has received support from RYC2021-031099-I and PID2021-123313NA-I00 of MICIN/AEI/10.13039/501100011033/FEDER,UE, NextGenerationEU/PRT. CT acknowledges the INAF grant 2022 LEMON. GD acknowledges support by UKRI-STFC grants: ST/T003081/1 and ST/X001857/1. MR acknowledges financial support from the INAF mini-grant 2022 ‘‘GALCLOCK’’.

DATA AVAILABILITY

The INSPiRE spectra used in this paper are publicly available through the ESO Phase 3 Archive Science Portal under the collection INSPiRE (https://archive.eso.org/scienceportal/home?data_collection=INSPiRE, <https://doi.eso.org/10.18727/archive/36>).

REFERENCES

- Adelman-McCarthy J. K., et al., 2006, *ApJS*, 162, 38
 Alarie A., Morisset C., 2019, *Rev. Mex. Astron. Astrofis.*, 55, 377
 Allen M. G., Groves B. A., Dopita M. A., Sutherland R. S., Kewley L. J., 2008, *ApJS*, 178, 20
 Ardila F., et al., 2018, *ApJ*, 863, 28
 Baldwin J. A., Phillips M. M., Terlevich R., 1981, *PASP*, 93, 5
 Barbosa C. E., Spiniello C., Arnaboldi M., Coccato L., Hilker M., Richtler T., 2021, *A&A*, 649, A93
 Belfiore F., et al., 2016, *MNRAS*, 461, 3111
 Bennett C. L., Larson D., Weiland J. L., Hinshaw G., 2014, *ApJ*, 794, 135
 Binette L., Magris C. G., Stasińska G., Bruzual A. G., 1994, *A&A*, 292, 13
 Buitrago F., Trujillo I., Conselice C. J., Bouwens R. J., Dickinson M., Yan H., 2008, *ApJ*, 687, L61
 Caldwell N., 1984, *PASP*, 96, 287
 Cid Fernandes R., Stasińska G., Mateus A., Vale Asari N., 2011, *MNRAS*, 413, 1687
 Ciesla L., Elbaz D., Fensch J., 2017, *A&A*, 608, A41
 D'Ago G., et al., 2023, *A&A*, 672, A17, INSPiRE DR2
 Daddi E., et al., 2005, *ApJ*, 626, 680
 Dopita M. A., Sutherland R. S., 1995, *ApJ*, 455, 468
 Dopita M. A., Massaglia S., Bodo G., Arnaboldi M., Merluzzi P., 2000, in Kastner J. H., Soker N., Rappaport S., eds, *Astronomical Society of the Pacific Conference Series Vol. 199, Asymmetrical Planetary Nebulae II: From Origins to Microstructures*. p. 423
 Elbaz D., et al., 2007, *A&A*, 468, 33
 Ferland G. J., Netzer H., 1983, *ApJ*, 264, 105
 Ferland G. J., et al., 2017, *Rev. Mex. Astron. Astrofis.*, 53, 385
 Ferré-Mateu A., Trujillo I., Martín-Navarro I., Vazdekis A., Mezcuca M., Balcells M., Domínguez L., 2017, *MNRAS*, 467, 1929
 Gallagher J. S., Bushouse H., Hunter D. A., 1989, *AJ*, 97, 700
 Greggio L., Renzini A., 1990, *ApJ*, 364, 35
 Groves B. A., Dopita M. A., Sutherland R. S., 2004, *ApJS*, 153, 75
 Gutkin J., Charlot S., Bruzual G., 2016, *MNRAS*, 462, 1757
 Halpern J. P., Steiner J. E., 1983, *ApJ*, 269, L37
 Kauffmann G., et al., 2003, *MNRAS*, 341, 54
 Kennicutt Jr. R. C., 1998, *ApJ*, 498, 541
 Kennicutt R. C., Evans N. J., 2012, *ARA&A*, 50, 531
 Kewley L. J., Dopita M. A., Sutherland R. S., Heisler C. A., Trevena J., 2001, *ApJ*, 556, 121
 Kewley L. J., Geller M. J., Jansen R. A., 2004, *AJ*, 127, 2002
 Kewley L. J., Groves B., Kauffmann G., Heckman T., 2006, *MNRAS*, 372, 961
 Kroupa P., Weidner C., 2003, *ApJ*, 598, 1076
 Kuijken K., 2011, *The Messenger*, 146, 8
 Kuijken K., et al., 2019, *A&A*, 625, A2
 La Barbera F., et al., 2019, *MNRAS*, 489, 4090
 Lee M.-Y. L., Yan R., Ji X., Algodon G., Westfall K., Lin Z., Belfiore F., Bundy K., 2024, *A&A*, 690, A83
 Maksymowicz-Maciata M., et al., 2024, *MNRAS*, 531, 2864
 Martín-Navarro I., et al., 2023, *MNRAS*, 521, 1408
 Martínez-Paredes M., Bruzual G., Morisset C., Kim M., Meléndez M., Binette L., 2023, *MNRAS*, 525, 2916
 Maseda M. V., et al., 2021, *ApJ*, 923, 18
 Melnick J., De Propriis R., 2013, *MNRAS*, 431, 2034
 Mendez R. H., Soffner T., 1997, *A&A*, 321, 898
 Morisset C., Delgado-Inglada G., Flores-Fajardo N., 2015, *Rev. Mex. Astron. Astrofis.*, 51, 103

- Morrissey P., et al., 2007, *ApJS*, 173, 682
- Murphy E. J., et al., 2011, *ApJ*, 737, 67
- Naab T., et al., 2014, *MNRAS*, 444, 3357
- Papaderos P., et al., 2013, *A&A*, 555, L1
- Plat A., Charlot S., Bruzual G., Feltre A., Vidal-García A., Morisset C., Chevillard J., Todt H., 2019, *MNRAS*, 490, 978
- Rola C. S., Terlevich E., Terlevich R. J., 1997, *MNRAS*, 289, 419
- Rosa-González D., Terlevich E., Terlevich R., 2002, *MNRAS*, 332, 283
- Roy N., et al., 2018, *MNRAS*, 480, 1057
- Salim S., 2014, *Serbian Astronomical Journal*, 189, 1
- Salvador-Rusiñol N., Beasley M. A., Vazdekis A., Barbera F. L., 2021, *MNRAS*, 500, 3368
- Salvador-Rusiñol N., Ferré-Mateu A., Vazdekis A., Beasley M. A., 2022, *MNRAS*, 515, 4514
- Sánchez S. F., et al., 2022, *ApJS*, 262, 36
- Scognamiglio D., et al., 2020, *The Astrophysical Journal*, 893, 4
- Spiniello C., et al., 2021a, *A&A*, 646, A28, INSPIRE Pilot
- Spiniello C., et al., 2021b, *A&A*, 654, A136, INSPIRE DR1
- Spiniello C., et al., 2024, *MNRAS*, 527, 8793
- Stasińska G., et al., 2008, *MNRAS*, 391, L29
- Sutherland R. S., Dopita M. A., 2017, *ApJS*, 229, 34
- Taniguchi Y., Shioya Y., Murayama T., 2000, *AJ*, 120, 1265
- Tortora C., et al., 2016, *MNRAS*, 457, 2845
- Tortora C., et al., 2018, *MNRAS*, 481, 4728
- Trujillo I., Conselice C. J., Bundy K., Cooper M. C., Eisenhardt P., Ellis R. S., 2007, *MNRAS*, 382, 109
- Trujillo I., Cenarro A. J., de Lorenzo-Cáceres A., Vazdekis A., de la Rosa I. G., Cava A., 2009, *ApJ*, 692, L118
- Trujillo I., Ferré-Mateu A., Balcells M., Vazdekis A., Sánchez-Blázquez P., 2014, *ApJ*, 780, L20
- Vazdekis A., Koleva M., Ricciardelli E., Röck B., Falcón-Barroso J., 2016, *MNRAS*, 463, 3409
- Vernet J., et al., 2011, *A&A*, 536, A105
- Yan R., Blanton M. R., 2012, *ApJ*, 747, 61
- Yan R., Newman J. A., Faber S. M., Konidaris N., Koo D., Davis M., 2006, *ApJ*, 648, 281
- de Jong J. T. A., et al., 2017, *A&A*, 604, A134
- van Dokkum P. G., et al., 2008, *ApJ*, 677, L5

This paper has been typeset from a $\text{\TeX}/\text{\LaTeX}$ file prepared by the author.